Reaction Chemistry & Engineering

ROYAL SOCIETY OF CHEMISTRY

PAPER

View Article Online
View Journal | View Issue

Cite this: *React. Chem. Eng.*, 2025, 10, 90

Kinetics of the valorization of hexoses with Sn-USY catalysts in methanolic media: glycosidation *vs.* retroaldol cleavage†

J. M. Jimenez-Martin,[a] M. El Tawil-Lucas,[a] C. García-Jerez,[a] J. Moreno,[a] A. García,[a] B. Hernández[a] and J. Iglesias *[ab]

Catalytic performance of potassium-exchanged Sn-containing USY zeolite ([K]Sn-USY) for the transformation of hexoses into methyl lactate in methanol has been studied. This work explores the effects of temperature and catalyst loading on this transformation process, shedding light on the kinetic aspects of this process in which the starting sugars undergo a complex network of different transformations to yield different biobased products with commercial interest. The proposed kinetic model integrates several key reactions: isomerization of the starting sugars, glycosidation with the alcohol solvent, retro-aldol cleavage of carbohydrates to minor sugars, and hydrolytic side transformations. By considering these steps, insights into the determining factors that influence overall transformation and high selectivity of the [K]Sn-USY zeolite for methyl lactate are clarified. Notably, this work highlights the formation of side products, including methoxy methyl 2-hydroxy-butanoate (MMHB) and glycolaldehyde dimethyl acetal (GADMA), which have been previously overlooked in other kinetic modelling and derived from the retroaldol cleavage of aldoses. The [K]Sn-USY catalysts exhibit promising activity and selectivity, making them attractive candidates for bio-based plastic production. A comprehensive understanding of the catalytic behavior and side product formation contributes to the optimization of these catalysts for sustainable carbohydrate valorization.

Received 25th June 2024,
Accepted 7th October 2024

DOI: 10.1039/d4re00307a

rsc.li/reaction-engineering

1. Introduction

Sn-containing zeolites represent a collection of versatile catalytic systems that demonstrate outstanding catalytic activities in various transformations, particularly in isomerization of sugars[1–3] and valorization of carbohydrates into valuable chemicals, including 5-(hydroxymethyl) furfural,[4,5] alkyl levulinates,[6] and lactic acid or alkyl lactates.[7–10] This versatility presents an advantage in the development of biorefinery models to produce several platform chemicals from biomass-derived carbohydrates. The aforementioned alkyl lactates are an interesting chemical platform for the production of bio-based and biodegradable plastic, such as poly-lactic acid (PLA),[11] production of which can be achieved *via* lactide, previously obtained by transesterification of alkyl lactates[12,13] and subsequent ring-opening polymerization.[14,15] These strategies introduce new possibilities to produce PLA based on catalytic pathways, increasing its selectivity and cascading the polymerization of lactic acid obtained by the fermentative process.[16]

Production of alkyl lactates from carbohydrates in an alcohol medium and in the presence of Lewis acid catalysts, such as Sn-containing zeolites, consists of a cascade reaction with several steps. Initially, glucose is isomerized to fructose (a ketose isomer of glucose), enabling the retroaldol cleavage of the C–C bonds between carbons 3 and 4, thereby leading to the formation of glyceraldehyde and dihydroxyacetone. Both trioses can be converted to methyl lactate (MLa); this undergoes dehydration to 2-hydroxyacrolein, which undergoes keto–enol tautomerism to produce pyruvaldehyde. This intermediate is then acetalized with an alcohol solvent to form a hemiacetal, which is readily isomerized through 1,2 hydride shift to yield the corresponding alkyl lactate.[17] Along these transformations, the production of a wide variety of side products is feasible, diminishing the yield towards the target alkyl lactate. Such side transformations include glycosidation or dehydration of the starting sugar substrate,[4,18] retroaldol cleavage of sugars in aldose form—yielding a tetrose and a diose—[19] or the acetalization of the hemiacetal.[17]

Identifying the optimal conditions of MLA production is challenging since the reaction involves numerous steps and employs highly versatile tin-containing zeolites. One approach lies in the development of kinetic models for Sn-Beta zeolites.

[a] *Chemical & Environmental Engineering Group, Universidad Rey Juan Carlos, C/Tulipán s/n. Móstoles, 28933, Madrid, Spain. E-mail: jose.iglesias@urjc.es; Tel: +34 914888565*
[b] *Instituto de Tecnologías para la Sostenibilidad, Universidad Rey Juan Carlos, C/Tulipán s/n. Móstoles, 28933, Madrid, Spain*

† Electronic supplementary information (ESI) available. See DOI: https://doi.org/10.1039/d4re00307a

Rajabbeigi *et al.*[20] covered the kinetic study of the isomerization between glucose, fructose and mannose in water between 70 and 130 °C, taking into account the deactivation of the catalyst in the kinetic model. Tosi *et al.*[21] conducted the evaluation of the conversion of glucose and fructose to methyl lactate at high temperature (160 °C), introducing the formation of methyl glycosides as side products at the beginning of the reaction. This work demonstrated sugar glycosidation is reversible under the tested conditions, and thus, glycosides act as masking agents of the substrate. Nevertheless, tin-containing zeolites with other structures are demonstrated to have different catalytic performances in the production of methyl lactate.[22,23] In those cases, faujasite structures remain scarcely studied despite providing outstanding catalytic activity and higher yields towards alkyl lactates than Sn-β. Under these circumstances, further research is needed to unravel the kinetics and reaction rates in each of the steps for this particular zeolite.

This research focuses on the study of the catalytic performance of a potassium-exchanged Sn-containing USY zeolite in the transformation of glucose, fructose and mannose in methanol media. The study explores the influence of the temperature conditions between 100 and 160 °C and the catalyst loading, covering both isomerization and retro-aldol cleavage promotion ranges, as well as different side transformations at low reaction times (below 120 min). To uncover the determining steps of this transformation, a kinetic model of the detected transformations is proposed. The model integrates for the first time the isomerization of the three sugars and the equilibria with their methyl glycosides, and the formation of side compounds, MLa promoted by Sn catalysts and compounds generated by retro-aldol reactions. Integration of all the reactions helps to determine the influence of the starting substrate, the operating temperature, and the catalyst loading under the operating space. Understanding the effects of these variables on the yields of each product is critical for advancing the development of K-exchanged Sn-USY catalysts.

2. Materials and methods

2.1. Materials

Commercial USY zeolite (CBV 712, Zeolyst International), nitric acid (HNO_3, Sigma Aldrich, 70%), methylene chloride (CH_2Cl_2, Scharlab), tin(IV) chloride pentahydrate ($SnCl_4{\cdot}5H_2O$, 98%, Alfa Aesar), and triethylamine ($N(CH_2CH_3)_3$, NEt_3, 99%, Sigma Aldrich) and potassium chloride (99%, Sigma Aldrich) were used in the synthesis of the catalyst. D-(+)-Glucose (GLU, 99%, Sigma Aldrich), D-(−)-fructose (FRU, 99%, Sigma Aldrich) and methanol (CH_3OH, HPLC Grade, Scharlab) were used in the catalytic tests as reaction substrates and solvent, respectively. Methyl D-lactate (MLA, 99%, Sigma Aldrich), methyl glycolate (MG, 98%, Sigma Aldrich), methyl vinyl glycolate (MVG, 98.4%, Apollo Scientific), glycolaldehyde dimethyl acetal (GADMA, 98%, Alfa Aesar), methyl levulinate (MLE, 98%, Sigma Aldrich), methoxymethyl furfural (MMF, 95%, abcr GmbH), hydroxymethyl furfural (HMF, 98%, abcr GmbH) and methyl 2-hydroxy-4-methoxybutanoate (MMHB, ≥95%, BioSynth) were used as standards for the calibration of GC, using decane ($C_{10}H_{22}$, 98%, Honeywell) as an internal standard. D-(+)-Glucose (GLU, 99%, Sigma Aldrich), D-(−)-fructose (FRU, 99%, Sigma Aldrich), D-(+)-mannose (MAN, 99%, Sigma Aldrich), methyl-D-glucopyranoside (MGP, 99%, Sigma Aldrich), methyl-D-mannopyranoside (MMP, 99%, Alfa Aesar) and methyl-D-fructopyranoside (MFP, 99%, Glentham Life Sciences) were all used as standards for sugars and glycosides quantification through gas chromatography, using Silyl-991 (BSTFA–TMCS, 99 : 1; Chromatography-Service) as derivatizing agent and malonaldehyde bis(diethyl acetal) (99%, Thermo-Scientific) as an external standard.

2.2. Catalyst preparation

The K-exchanged Sn-functionalized USY zeolite ([K]Sn-USY) was synthesized following a previously reported method,[23] involving a post-synthetic modification of a commercially available zeolite. The USY zeolite, commercially available, underwent calcination at 550 °C for 6 hours to remove NH_4^+ counterions before being treated with a nitric acid aqueous solution ($[HNO_3]$ = 10 mol L^{-1}) for 1 hour, extracting aluminum from the zeolite structure and creating vacancies. The acid dealumination step was repeated twice to ensure maximum removal of aluminum. Afterwards, the zeolite was dried by distilling off water from a methylene chloride suspension of the dealuminated zeolite, under inert atmosphere conditions, and using a Dean Stark apparatus for solvents heavier than water. $SnCl_4$ was then added to the CH_2Cl_2 zeolite suspension, to bind the tin atoms into the created aluminum vacancies. For this purpose, triethylamine was used as a catalyst to promote the grafting process. The Sn-functionalized zeolite was recovered by filtration and calcined at 550 °C for 6 hours in static air conditions. Finally, the tin-containing zeolite underwent ion exchange with a KCl aqueous solution ([KCl] = 0.5 M) for 2 hours, followed by a final calcination for 6 hours at 550 °C.

2.3. Catalyst characterization

The metal content in the [K]Sn-USY catalyst was determined using ICP-OES with a Varian Vista AX. Zeolite samples (0.1 g) were dissolved with a mixture of hydrofluoric and sulfuric acid (10 : 2 v/v). The suspension was heated until evaporation of HF and subsequently diluted in deionized water prior to its analysis. Textural properties of the porous catalyst were assessed through argon adsorption–desorption isotherms recorded at −186 °C, employing a Triflex unit (Micromeritics Corp.). The zeolite samples were subjected to an outgassing process, prior to their analysis, involving two steps. The first was conducted *ex situ*, applying 0.03 Torr vacuum and heating at 150 °C for 15 hours. The second outgassing step was conducted *in situ* (in the analysis port of the TriFlex unit), under vacuum (10^{-6} Torr), heating the samples at a 300 °C for 5 hours. The surface area was calculated using the B.E.T. equation, and the total pore volume was assumed to be recorded at P/P_0 = 0.95. X-ray powder diffraction (XRD) patterns were collected using a Philips X-Pert diffractometer with the Cu Kα line in the 2θ angle range from 5° to 90° (step size of 0.04°). DR-UV-vis spectra were recorded at

room temperature using a Cary 500 unit (Varian) equipped with a Praying Mantis™ accessory and a catalytic chamber (HVC-DRP, Harrick Scientific Products, NY) to perform *in situ* thermal treatments under controlled atmosphere conditions. Samples were preconditioned by heating at 200 °C under N_2 flow (70 mL g^{-1}) for 1 hour. The characterization of the environment of tin sites was assessed by means of SS MAS NMR using a Bruker AVANCE III HD-WB-400 MHz, operating with a constant magnetic field intensity B_0 of 9.4 T, fitted with a 4 mm NMR rotor. Acidity measurements were performed by temperature-programmed desorption of NH_3 in a Micromeritics 2910 (TPD/TPR) apparatus fitted with a TCD detector.

2.4. Evaluation of catalytic performance in methyl lactate synthesis

The assessment of the catalytic performance of the prepared [K]Sn-USY was performed in a 100 mL stainless steel reactor (MiniReactor Series; Autoclave Engineers; USA) equipped with a sample collector cooled with water to enable the periodic withdrawal of samples. The stirring and temperature conditions were controlled with the corresponding PID controllers (TTM-005; Toho Electronics; Japan). Typically, the substrate, the catalyst, the internal standard and methanol were placed together in the reactor vessel and sealed before setting the temperature to 150 °C and 500 rpm as stirring speed. After reaching the settled temperature, time zero is considered, withdrawing samples at 0, 5, 10, 30, 50, 80 and 120 minutes. All samples were filtered with 0.22 μm filters prior to analysis.

2.5. Samples analysis

The reaction samples were analyzed by means of gas chromatography. The analysis and quantification of sugar-derived products formed during the reaction were

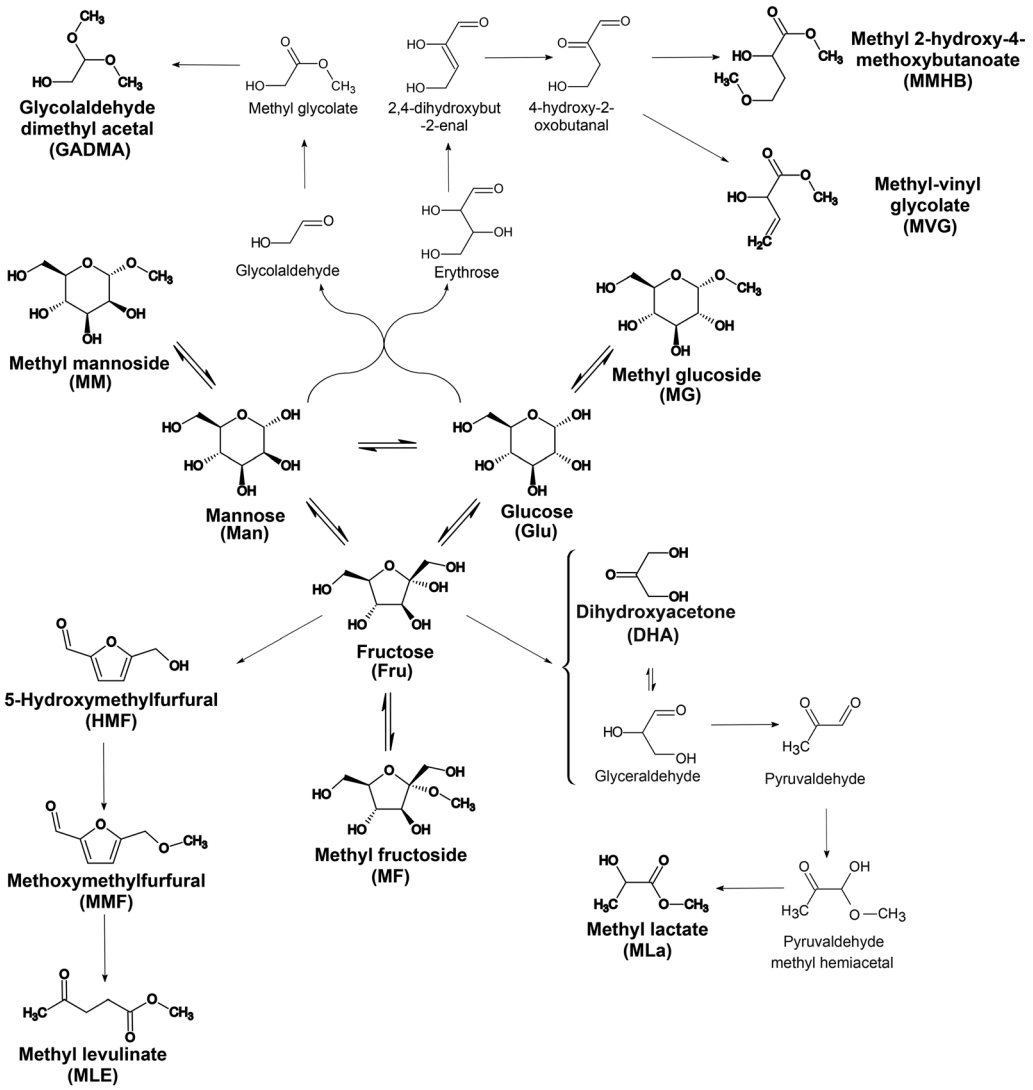

Fig. 1 Reaction scheme describing the different reaction routes present when treating C6 sugar monosaccharides in the presence of [K]Sn-USY in methanol medium.

performed with a Varian CP3900 GC unit fitted with a CPWAX-52-CB column and an FID detector. For the analysis of sugars and sugar glycosides, the samples were first treated by silylation, according to the procedure described by F. Pienkoß *et al.*[24] using BFTSA as a derivatization agent. Derivatized samples were analyzed with a Varian CP3900 GC unit fitted with an HP-1 column and an FID detector. Both chromatographs were previously calibrated using standard stock solutions of the identified reaction products with known concentrations. Substrate conversion (X_i) and product yields (Y_i) were calculated using eqn (1) and (2), respectively.

$$X_i\,(\%) = \frac{\text{reacted moles of substrate}}{\text{initial moles of substrate}} \cdot 100 \quad (1)$$

$$Y_i\,(\%) = \frac{\text{moles of product } i}{\text{initial moles of substrate } i \cdot \text{stoichiometric coefficient}} \cdot 100 \quad (2)$$

In eqn (2), the stoichiometric coefficient refers to the number of carbon atoms of the starting substrate divided by the number of carbon atoms of the considered product.

2.6. Kinetic modelling

2.6.1 Reaction network. The transformation of the hexoses – glucose, mannose or fructose – in methanol media, and in the presence of bifunctional Brønsted–Lewis acid catalysts provides a set of products that can be classified into four types of chemicals: I) free sugars, comprising glucose (Glu), mannose (Man) and fructose (Fru); II) methyl glycosides, which are evolved from the etherification of the free sugars with the alcohol solvent (MG, MM, MF); III) C2, C3 and C4 carbon backbone compounds (GADMA, DHA, MLa, MVG and MMHB), being produced through the retro-aldol cleavage of sugars; and IV) furanics (5-HMF, MMF, MLe), which are evolved through hydrolytic transformations of fructose. The reaction scheme representing all the transformations yielding these products is depicted in Fig. 1.

The reaction system comprises the Lewis-acid catalyzed isomerization between the three hexoses (glucose, mannose and fructose) together with their equilibria with methyl glycosides (Brønsted acid catalyzed), which act as substrate-masking agents during lactate synthesis.[21] Apart from the equilibrium transformations between sugars and their corresponding methyl glycosides, the following irreversible transformations take place: Retro aldol condensation reactions (Lewis acid driven) occur from all the free sugars. In the case of aldoses (mannose and glucose), this splitting occurs in an asymmetric way, conducting a C2-fragment (glycolaldehyde) and a C4-sugar (tetrose). The former, undergoes a double acetalization in the methanol medium, finally providing glycolaldehyde dimethyl acetal (GADMA), whereas the latter evolves through a cascade of transformations to provide two different products through parallel transformations: methyl vinyl glycolate (MVG) and 4-methoxy, 2-hydroxy methyl butanoate (MMHB). Regarding the retro-aldol cleavage of fructose, the symmetric splitting of the molecule provides 2 C3 carbon backbone moieties: dihydroxyacetone (DHA) and glyceraldehyde (GLA), which are in equilibrium. GLA undergoes a cascade of transformations involving dehydration, tautomerization and 1,2-H shift processes that lead to MLa. Finally, a last reaction route is also present, in which fructose evolves through a Brønsted-acid catalyzed pathway to yield 5-hydroxymethyl furfural (HMF), its methyl ether (MMF), and the result from the hydrolytic transformation to methyl levulinate (MLe).

2.6.2 Model development. Bearing in mind the previous transformation of the tested hexoses in the methanol medium, a simplified version of the detailed reaction scheme is proposed in Fig. 2. Based on this scheme we have formulated a pseudo-homogeneous kinetic model to describe the rate of the transformation of hexoses in the presence of [K]Sn-USY.

The system proposed simplifies the whole mechanism to match the conclusions arising from the preliminary analysis of the experimental results. The epimerization of aldoses has been described to be more difficult than their isomerization into ketoses but occurs under the same conditions as sugar isomerization. Thus, epimerization of aldoses has been

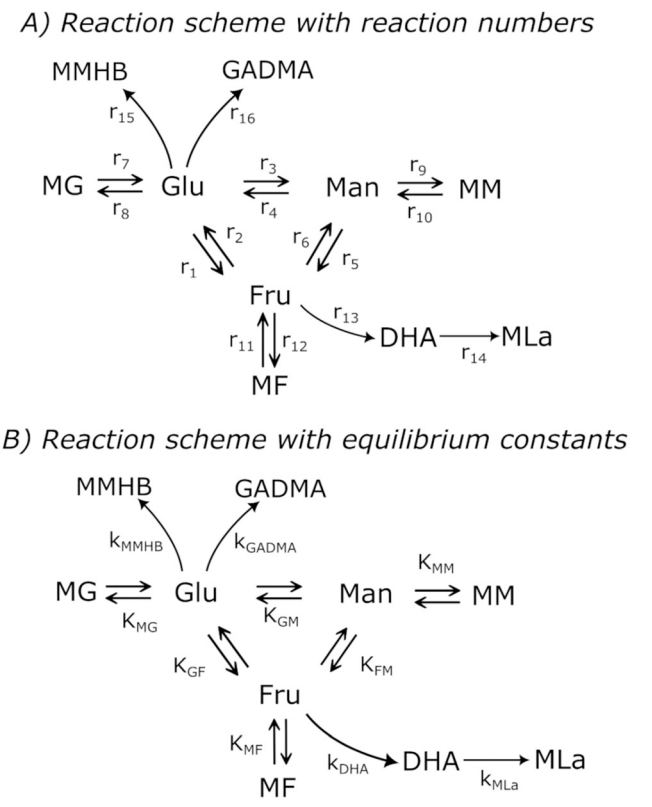

Fig. 2 Simplified reaction scheme with its A) reactions and B) their kinetic and equilibrium constants in the transformation of hexoses with [K]Sn-USY in methanol.

Table 1 Summary of the kinetic model equations

Component	Equation	Eqn
Glucose	$\frac{dC_G}{dt} = \frac{m_{cat}}{V_{react}}\left[-k_1\left(C_G - \frac{C_F}{K_{FG}}\right) + k_4(C_M - K_{FG}K_{MF}C_G) + k_7\left(C_{MG} - \frac{C_G}{K_{G-MG}}\right) - k_{MMBH}C_G - k_{GADMA}C_G\right]$	(3)
Methyl glucoside	$\frac{dC_{MG}}{dt} = \frac{m_{cat}}{V_{react}}\left[-k_7\left(C_{MG} - \frac{C_G}{K_{G-MG}}\right)\right]$	(4)
Mannose	$\frac{dC_M}{dt} = \frac{m_{cat}}{V_{react}}\left[-k_4(C_M - K_{FG}K_{MF}C_G) + k_6\left(C_G - \frac{C_M}{K_{MF}}\right) - k_9\left(C_M - \frac{C_{MM}}{K_{MM-M}}\right)\right]$	(5)
Methyl mannoside	$\frac{dC_{MM}}{dt} = \frac{m_{cat}}{V_{react}}\left[k_9\left(C_M - \frac{C_{MM}}{K_{MM}}\right)\right]$	(6)
Fructose	$\frac{dC_F}{dt} = \frac{m_{cat}}{V_{react}}\left[k_1\left(C_G - \frac{C_F}{K_{FG}}\right) - k_6\left(C_G - \frac{C_M}{K_{MF}}\right) + k_{11}\left(C_F - \frac{C_{MF}}{K_{F-MF}}\right) - k_{DHA}\cdot C_F\right]$	(7)
Methyl fructoside	$\frac{dC_{MF}}{dt} = \frac{m_{cat}}{V_{react}}\left[-k_{11}\left(C_F - \frac{C_{MF}}{K_{MF}}\right)\right]$	(8)
DHA	$\frac{dC_{DHA}}{dt} = \frac{m_{cat}}{V_{react}}[k_{DHA}\cdot C_F - k_{MLa}\cdot C_{DHA}]$	(9)
MLa	$\frac{dC_{MLa}}{dt} = \frac{m_{cat}}{V_{react}}[k_{MLa}\cdot C_{DHA}]$	(10)
DAGMA	$\frac{dC_{DAGMA}}{dt} = \frac{m_{cat}}{V_{react}}[k_{GADMA}C_G]$	(11)
MMHB	$\frac{dC_{MMHB}}{dt} = \frac{m_{cat}}{V_{react}}[k_{MMBH}C_G]$	(12)

considered within the kinetic model. Regarding the complex series of transformations conducted to the different α-hydroxy esters (MLa, MVG, MMHB), most of the reaction intermediates have not been detected in quantifiable amounts, probably as a consequence of a low lifetime due to their large reactivity under the tested reaction conditions. In this way, these series of transformations have been lumped into a single transformation, with a kinetic rate corresponding to one of the limiting stages. This has been applied to GADMA and MMHB, which both are assumed to be directly produced from glucose. The equilibrium between glucose and mannose favors the formation of glucose so these products are only assumed to be generated from glucose. The formation of MVG is too low as compared to that of MMHB, so it is assumed negligible, and it was removed from the reaction scheme shown in Fig. 2. In a similar way, the cascade of transformations conducting to methyl lactate is lumped into a series of two reactions, one conducting to dihydroxyacetone from fructose, and a second one from DHA to methyl lactate. Finally, Brønsted acid-promoted reactions such as the dehydration of fructose into 5-hydroxymethyl furfural, and its subsequent hydrolytic transformation into methyl levulinate and methoxy methyl furfural are not included since the production rate is very small.

Taking into account these assumptions, a pseudo-homogeneous first-order kinetic model has been proposed with the equations summarized in Table 1. Eqn (3) to (5) reproduce the decomposition and formation of sugars. In the isomerization equilibria the equilibrium constants, defined as given in Table 2, must meet $K_{GF}K_{GM}K_{FM} = 1$. Thus, K_{GM} can be substituted in the eqn (3) and (5) by $K_{GM} = 1/(K_{FG}K_{MF})$. The resultant equilibrium constants, K_{FG} and K_{MF}, are determined fitting the van't Hoff equation, eqn (13), to the reported thermodynamic data,[25,26] see more details in the ESI.† Eqn (4), (6) and (8) define the formation and decomposition of methyl glycosides. The formation of these methyl glycosides is defined by the kinetic parameter of the reactions and the equilibrium with their corresponding sugar. For these reactions, no thermodynamic data is available so the equilibrium constants are determined by fitting them using the experimental data. The definitions of all the thermodynamic constants with the kinetic ones are provided in Table 2. Even though these equilibrium constants are mostly driven by the reaction's thermodynamics, it is important to note that they are also affected by the adsorption of each component on the zeolite.

$$K_{ij} = \exp\left(-\frac{\Delta H^0}{RT} + \frac{\Delta S^0}{R}\right) \quad (13)$$

Table 2 Definition of equilibrium constants from kinetic constants

Equilibrium constant	Eqn
$K_{FG} = \frac{k_1}{k_2}$	(14)
$K_{GM} = \frac{k_4}{k_3}$	(15)
$K_{MF} = \frac{k_6}{k_5}$	(16)
$K_{MM-M} = \frac{k_9}{k_{10}}$	(17)
$K_{G-MG} = \frac{k_7}{k_8}$	(18)
$K_{F-MF} = \frac{k_{11}}{k_{12}}$	(19)

Apart from the equilibria, the formation of MLa follows a chain reaction mechanism with DHA as an intermediate as described in eqn (9) and (10). Two side products are included in the model: GADMA, which is generated from fructose as shown in eqn (11); and MMHB, which is generated as presented in eqn (12). The kinetic constants obtained for MLa, DHA, GADMA and MMHB include the effect of mass transfer, but this is negligible since the zeolites have particle sizes in the order of micrometers and the reactor is magnetically agitated at 500 rpm.

Kinetic parameters are related to the Arrhenius equation, eqn (20). The kinetic model was implemented in Python utilizing the optimization framework *Pyomo*. In the model, the differential equations are implemented following an orthogonal collocation method with the *Pyomo.dae* library. The objective function was defined as the minimization of the sum of residual squares (SSE), see eqn (21). The non-linear programming problem that defines the model was solved with *Ipopt v.3.11* as the solver.

$$k_i = k_{i,0} \cdot e^{\left(\frac{-E_{Ai}}{RT}\right)} \tag{20}$$

$$\mathrm{SSE} = \sum_{i=1}^{I}\sum_{m=1}^{M}\sum_{n=1}^{N}\left(C_{i,m,n}^{\mathrm{experimental}} - C_{i,m,n}^{\mathrm{model}}\right)^2 \tag{21}$$

3. Results and discussion

3.1. Catalyst characterization

The [K]Sn-USY catalyst prepared through the post-synthetic modification of a commercial USY zeolite presents nearly the same XRD patterns as that of the parent material through the different stages of its preparation (Fig. 3A), suggesting that the zeolite preserves its crystallinity with minor or no changes in the zeolitic structure. Argon adsorption–desorption isotherms (Fig. 3B) also reveal that the tin-functionalized material was scarcely modified. Ion exchange zeolite is featured by an adsorption–desorption isotherm, which seems a combination of types I and IV. This suggests the presence of micropores, corresponding to the zeolite contribution, with increased adsorption capacity in the P/P_0 middle region (P/P_0 = 0.5–0.7), which is caused by mesopores. This slight increase of mesoporosity is attributed to the partial dissolution of the zeolite during dealuminations, which might cause additional mesoporosity to that shown by the parent material (USY). The final zeolite also presents an H4 hysteresis loop on its argon adsorption–desorption isotherm, which could be attributed to the condensation of argon in the interparticular voids of the sample and mesopores.

The total metal loading found in the functionalized zeolite by ICP-OES analysis accounted for 1.91 wt%. This result evidences the high efficiency of the metalation step, since almost quantitative incorporation of the tin added in this synthesis stage was achieved, as the theoretical tin loading to be achieved was 2.00 wt% Sn in the final material. This high efficiency is ascribed to a combination of the efficient dealumination step, which creates plenty of framework vacancies, and the high effectiveness of the triethylamine-driven metal grafting. Contacting the tin-functionalized zeolite with a KCl aqueous solution led to the incorporation of 0.4 wt% of potassium into the catalyst. This process exerts an important effect on the reduction of the total acidity of the catalyst, especially of strong Brønsted acid sites with ion exchange capacity. The result is a catalyst with a reduced Brønsted acid capacity, but with noticeable Lewis acidity, coming from the attached Sn species. However, the obtained material still presents a B/L = 9. This indicates that, despite the selective reduction of Brønsted acidity, mainly attributed to the remaining acid protons acting as tetrahedral aluminum compensating ions, which are not fully neutralized. The main reason seems that the remaining

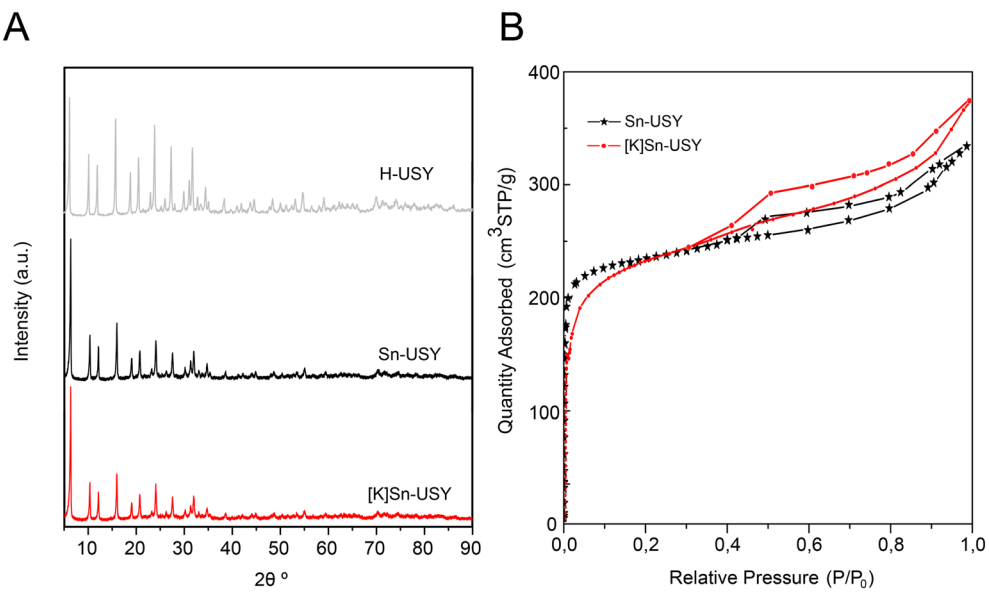

Fig. 3 A) XRD patterns and B) argon adsorption–desorption isotherms, recorded for the [K]Sn-USY catalyst.

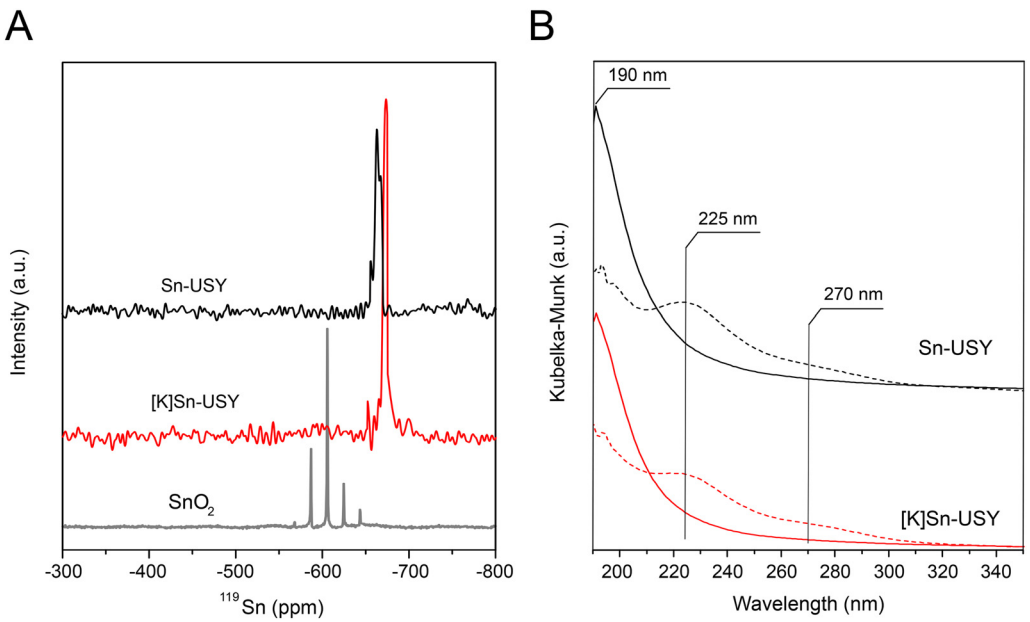

Fig. 4 A) ^{119}Sn solid-state MAS NMR and B) DR UV-vis analyses recorded for the [K]Sn-USY catalyst.

Brønsted acidity can be ascribed to the presence of unoccupied silanol nests, with weaker Brønsted acidity. Nevertheless, the obtained catalyst presents a Lewis-enhanced acidity and an expected improved performance on hexose transformation.

The environment of the zeolite-attached metal sites was evaluated through ^{119}Sn solid-state MAS NMR and DR UV-vis analysis, the results are depicted in Fig. 4. ^{119}Sn NMR spectra recorded for Sn-USY and its K-exchanged counterpart are depicted in Fig. 4A. These spectra feature main signals located at −660 ppm in the case of Sn-USY and at −670 ppm for [K]Sn-USY. Both signals are located in the region commonly ascribed to the presence of hydrated tin sites in tetrahedral conformation. Besides, the lack of signals around −600 ppm points to the absence of large SnO_2 domains. The DR UV-vis spectra recorded for all the prepared materials, depicted in Fig. 4B, support the above conclusion on the absence of large domains of tin oxide. DR UV-vis spectrum recorded for the [K]Sn-USY catalyst presents a maximum absorption signal at 225 nm, together with a shoulder at 270 nm, both signals being conventionally ascribed to the presence of penta- and hexa-coordinated tin species. This result might be considered evidence for the presence of tin oxide species, but the removal of these signals when drying the sample under a vacuum at 300 °C points to an opposite direction. The spectra recorded for the dried sample are featured by a predominant signal located at 190 nm, corresponding to the ligand-to-metal charge transfer in tin species with tetrahedral coordination incorporated into the zeolite framework.[27] In this way, the signals detected in the [K]Sn-USY exposed to the atmosphere humidity can be easily ascribed to hydrated tin sites, in which water acts as ligands, expanding the coordination sphere of the metal centers.[28]

From the previous results it can be concluded that the prepared catalysts display the right combination of textural and structural physicochemical properties together with the right functionalization degree with tin species in tetrahedral coordination, which provide Lewis acidity to the final zeolitic catalysts, and thus, these are expected to show a high catalytic performance in the transformation of C6 sugars into methyl lactate, as reported elsewhere.[29]

3.2. Catalytic activity for the transformation of C6 sugars into methyl lactate

The catalytic activity of the [K]Sn-USY catalyst was assessed in the transformation of different hexoses (glucose, mannose and fructose) in the methanol medium under different temperatures and catalyst loading conditions. Results from tests conducted at different reaction temperatures for different sugar substrates are depicted in Fig. 5.

Reaction profiles suggest that both the isomerization of the different substrates and the etherification of free sugars to the corresponding methyl glycosides proceed at fast reaction rates, as it can be inferred from the high yields obtained towards these products during the early beginning of the reaction tests. Obviously, the temperature conditions strongly influenced the formation of these initial sugar derivatives, but at low-temperature conditions, the formation of methyl fructoside becomes the dominant reaction pathway, regardless of the starting substrate. As a consequence, maximum yields of MF (ranging from 60–80% of the starting free sugar) were produced after 120 min operating at 120 °C. Lower temperature conditions (100 °C) also produced methyl fructoside as the main product, though at slower reaction rates. Surprisingly, the formation of other glycosides (methyl glucoside, methyl mannoside) was quite

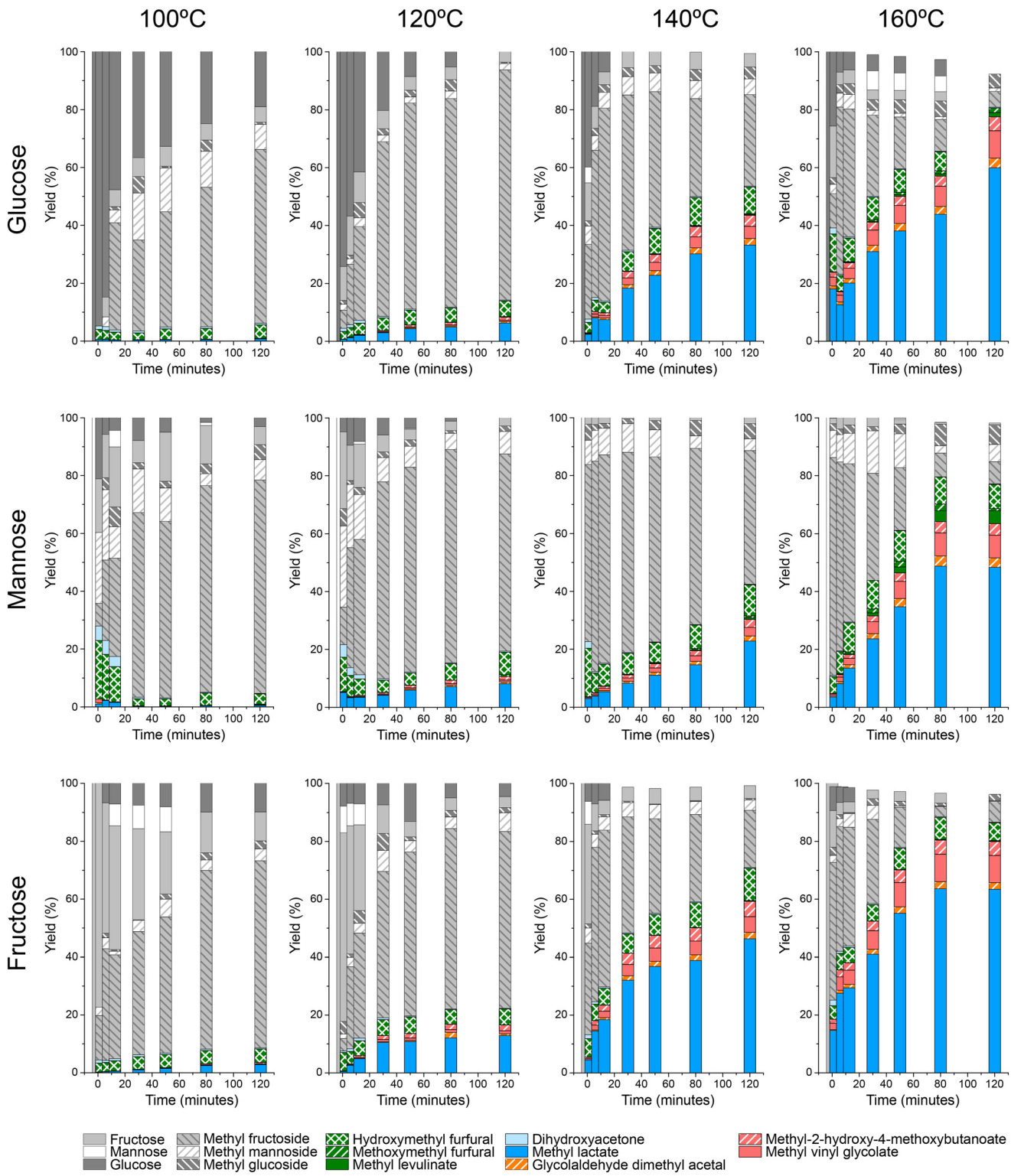

Fig. 5 Results from the transformation of glucose, mannose and fructose in the presence of the [K]Sn-USY catalyst performed at different temperature conditions (100–160 °C). Reaction conditions: substrate loading = 0.26 mol L^{-1}; catalyst loading = 0.4 g; reaction time = 120 min.

reduced, indicating that the formation of fructose, and its etherification with the alcohol solvent is prevalent. This result suggests that the isomerization of the starting monosaccharide occurred at a substantially faster rate than glycosidation reactions, as it can be easily estimated from the abrupt consumption of all the sugar substrates during the first stages of the reaction tests. Among the glycosidation reactions, the higher productivity of methyl fructoside as

compared to mannoside and glucoside suggests that the formation of the former is dominant. This different reactivity might be caused by differences in the ring closure step of the Fischer–Helferich glycosidation mechanism between aldoses and ketoses, which could be easier for the latter, thus enhancing their reactivity in this transformation.[30] Finally, regarding the transformation of aldoses, the low productivity of glucose and mannose, or their methyl glycosides, when starting from mannose and glucose, respectively, suggest that epimerization reactions occur with very low extension, at least under the tested reaction conditions.

When considering higher temperature conditions, a substantial increase in the extension of parallel transformations to those previously described is observed. These other reactions include both the hydrolytic transformation of sugars to provide 5-HMF and its derivatives and the retro-aldol cleavage of sugars. Under these conditions, the production of methyl lactate becomes more dominant insofar as the reaction temperature increases, being produced in a higher extension at 160 °C and long reaction times (2 h) and reaching product yields in the range of 55–70%, depending on the starting substrate. Together with MLa, other products are also obtained, such as GADMA, MVG and MMHB, though in a limited extension – up to a yield of 2.3% for GADMA, 9.4% for MVG and 4.8% for MMHV, when treating fructose at 160 °C. On the other hand, hydrolytic pathways conducting to HMF, MMF and MLE, provide yields below 10% of the starting sugar in every case, because of the depressed Brønsted activity of [K]Sn-USY catalysts through ion exchange prevents these reactions.[22] No great differences can be found in terms of product distributions when using the different hexose substrates, though in the case of fructose, faster production of MLa, even at lower temperature conditions was observed. This is an expected result, as the cleavage of fructose into trioses, finally yielding MLa, does not require the isomerisation stage, as it occurs for glucose or mannose.

The evaluation of the influence of the catalyst loading was performed by studying this parameter at three different levels. For this purpose, the reaction temperature was fixed at 140 °C, and the catalyst loading was varied between 0.2 and 0.8 g (substrate to catalyst mass ratio 2.5–9.5 wt/wt). The results from these experiments using glucose, mannose and fructose as starting sugar substrates are depicted in Fig. 6.

The main products obtained in the presence of different catalyst loadings were all the same as already described. The results evidenced the expected trend, that the higher the catalyst loadings the faster the transformation of sugars and the production of final compounds such as MLa. This can be easily inferred from the fast consumption of the starting monosaccharides during the early stages of the tests and the increasing MLa yields, and related products, obtained at longer reaction times as the catalyst loading increased. From the kinetic profiles, it is observed that the addition of increasing quantities of the catalyst produced no great differences in the product distributions, further than the transformation of the starting sugars and intermediates progressed towards the formation of methyl lactate and similar products. Besides, the relationship between the catalyst loading and the extension of the different chemical transformations seems to be linear, prompting the absence of external mass transfer control of the transformation. Finally, the slight differences in terms of reactivity between the different substrates were the same as already described when evaluating the influence of temperature. Here again, fructose was converted in a faster way as compared to glucose and mannose, whereas this last (mannose) evidenced a less reactive behavior.

3.3. Kinetic modeling

The kinetic model determines the kinetic parameters that minimize the sum of square errors. The pre-exponential parameter and activation energies for the kinetic constants are provided in Table 3. The enthalpy and entropy values of the van't Hoff equation determined from the kinetics for the equilibria between the sugars and their methyl glucosides are reported in Table 4. Analyzing the obtained equilibrium constants, it is observed that K_{G-MG} has values between 0.1 and 0.3 and for K_{M-MM} the values estimated are between 3 and 8. In both equilibria, this highlights the isolating effect of methanol for both sugars. This is particularly relevant in the case of glucose, where it avoids the decomposition into MMHB and DAGMA. On the other hand, K_{F-MF} has a value around 1, suggesting that the equilibrium between both components is quite similar.

This can also be observed in the evolution of the concentration of different substrates (mannose, fructose, and glucose) reported in Fig. 7 to 9. From the equilibrium between the sugars, it is observed that the degradation of mannose is promoted, which is in line with the observation of Tosi *et al.*[21] In the equilibria of the sugars with the methyl glycosides, it can be seen that the isolation affects them with an increase of the concentration followed by a later drop. The comparison of the experimental values with the values reported for the equilibrium constants shows the expected behavior for MM and MG, but for MF the value obtained for K_{F-MF} is around 1, and the concentration of MF is between 3 and 5 times higher than the one of fructose. This lower value obtained differs from the experimental observation since the thermodynamic equilibrium constant introduced for the sugar's equilibria has been modeled as in other previous works and it is only based on reaction thermodynamics. Other phenomena such as the adsorption of the sugars and methyl glycosides on the catalyst modify the equilibrium and the partition coefficients related to that adsorption are included within the obtained equilibrium constant. Future studies focusing on interphase characterization can provide further knowledge to decouple such phenomena. Similarly, future work can be carried out comparing other alcohol

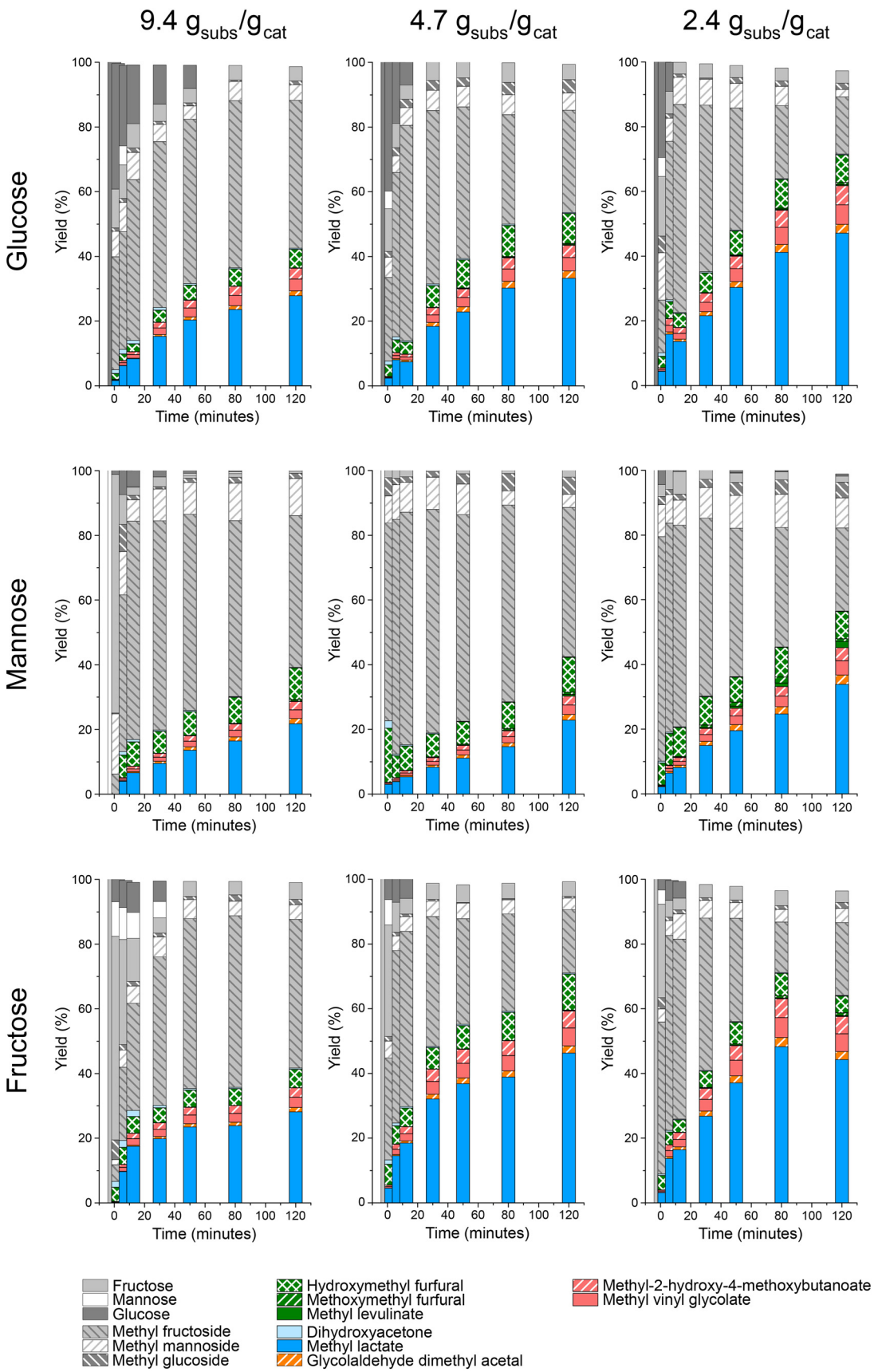

Fig. 6 Results from the transformation of glucose, mannose and fructose in the presence of the [K]Sn-USY catalyst performed with different catalyst loadings (substrate : catalyst = 2.5–9.5 wt/wt). Reaction conditions: substrate loading = 0.26 mol L^{-1}; temperature = 140 °C; reaction time = 120 min.

Table 3 Summary of the parameters of the Arrhenius equation for the kinetic parameters. The error provided for each parameter corresponds to the maximum error observed between one experiment and the parameter estimated with all the experiments at the same time. Note that the value of the pre-exponential parameter and the activation energy cannot be negative, and the maximum value only applies in its positive form

Parameter	Pre-exponential parameter, k_o (L kg_{cat}^{-1} min^{-1})	Activation energy, E_a (kJ mol^{-1})
k_1	$7511 \pm 6.22 \times 10^8$	20.285 ± 54.212
k_4	$2.7 \times 10^{-12} \pm 26\,651$	38.963 ± 52.878
k_6	$8884 \pm 7.01 \times 10^4$	22.020 ± 20.02
k_7	$2.73 \times 10^{-9} \pm 28.08$	7.681 ± 10.08
k_9	$2.582 \times 10^{-16} \pm 1.7 \times 10^5$	2.726 ± 45.03
k_{11}	$264.232 \pm 4.1 \times 10^6$	27.360 ± 35.3
k_{DHA}	$3.382 \times 10^5 \pm 2.8 \times 10^9$	78.184 ± 7.194
k_{MLa}	$5.289 \times 10^8 \pm 3.1 \times 10^{12}$	103.877 ± 5.801
k_{GADMA}	$15.822 \pm 6.7 \times 10^6$	40.208 ± 44.58
k_{MMHB}	$7.761 \times 10^{11} \pm 2.18 \times 10^{19}$	142.031 ± 189.98

Table 4 Summary of parameters of the van't Hoff equation for the equilibrium constants between the sugars and their methyl glycosides. Note that the van't Hoff parameters for the equilibria between the sugars are based on previously reported data and are not determined

Equilibrium constant, K_{eq}	ΔS (J mol^{-1} K^{-1})	ΔH (kJ K^{-1})
K_{F-MF}	−297.63	−118.04
K_{G-MG}	52.38	26.169
K_{M-MM}	306.06	111.28

moieties through molecular design and molecular simulation could provide an initial guess of the entropy value to be used in the van't Hoff equation for the methyl glycosides. The value obtained for the entropy through correlations is higher than expected. On the contrary, the value for enthalpy is one order below that obtained for the reactions in the glycosides equilibria, something that can be expected.

Apart from the comparison of the equilibrium constants, the kinetic parameters were obtained. The activation energies estimated from the model for the methyl glycosides are around one order below those involved in the reactions corresponding to the equilibria between the sugars.

These great values are due to the high mixing rates of the reactor. At larger scales where mixing is not that efficient, the kinetic rates in the formation of methyl glycosides are expected to drop due to the mass transfer limitations. Apart from these limitations in the application of the model, it is also worth noting the errors are involved in the estimation of the kinetic parameters. Only three sets of experiments, each of them also with different initial substrates, have been employed in the estimation of the kinetic parameters, which implies the involvement of low information and subsequently large errors. Furthermore, the model proposed includes more terms than other approaches, which results in some parameters being cross-linked. As a result, there are some case studies where the activation energy obtained is slightly higher than double the one obtained by fitting all the experimental results together, which is the one reported as the average value.

The analysis of the kinetics for the two side products, MMHB and GADMA, show in both cases higher activation energies than the ones obtained for the methyl glycosides and the sugars equilibria. From both compounds, the one with the smaller activation energy is GADMA, but this energy is still double the one for the formation of mannose and fructose. This remarks that the preferred reaction paths for glucose are the transformation to fructose and methyl glucoside. Furthermore, at low temperatures, the formation of these reactions is preferred as it is shown in the concentration profiles reported in the ESI.† Thus, at these low temperatures, it is important to have methanol as an isolating agent since it can significantly help more on avoiding the formation of undesired compounds such as MMHB and DAGMA. In the case of glucose being employed as a substrate, it is partially stored in the form of MG and then it is released back to glucose for its transformation into fructose; see the profiles of MG in Fig. 6 to 8. Despite the prediction of the model, it does not ensure a good accuracy for these compounds at 140 °C and 160 °C, it can be observed that at low temperatures, 100 °C and 120 °C, the model perfectly fits the concentration, see figures reported in the ESI.† At low temperatures, the concentration of these compounds is higher, so it finally has a higher weight on the minimization of the square errors. Furthermore, it is also important to note that in the model, all retro-aldol reactions are included as a single one.

The kinetic parameters of MLa show that its formation is faster than the other two side products of the reaction system, GADMA and MMHB. The estimated activation energies are higher than those for the methyl glycosides and sugars equilibria, but the pre-exponential parameter is several orders higher. This indicates that the formation of MLa is more sensitive to the temperature and can be promoted by increasing it. The estimated kinetic parameter for MLa is also around 5 times higher than the one for the formation of the two other side products, GADMA and MMHB.

However, its generation is mostly promoted thanks to the formation of methyl glycosides as the isolating agents. This enhancement makes the system achieve a yield in the range of 0.25–0.3 mol L^{-1}, see results at 160 °C in the ESI.† This maximum yield is lower when mannose is the original substrate, ~0.2 mol L^{-1}, than for fructose and glucose. The transformation of mannose derives from other side products (MMHB and GADMA) and favors the accumulation of fructose as MF. Apart from the analysis of the parameters in MLa production, the comparison of the model with the experimental data shows that the two steps defined in the model are not always observed in the experimental data. At low temperatures, the experimental data in the formation of MLa follows the profile of a first-order mechanism, but the model is still in the first part of the profile, see ESI.† This leads to an error in predicting the concentration of MLa at low temperatures, but at high temperatures, the error is reduced. However, it is important to note the concentration achieved in each case. At low temperatures, the yield of MLa is below 5 mol

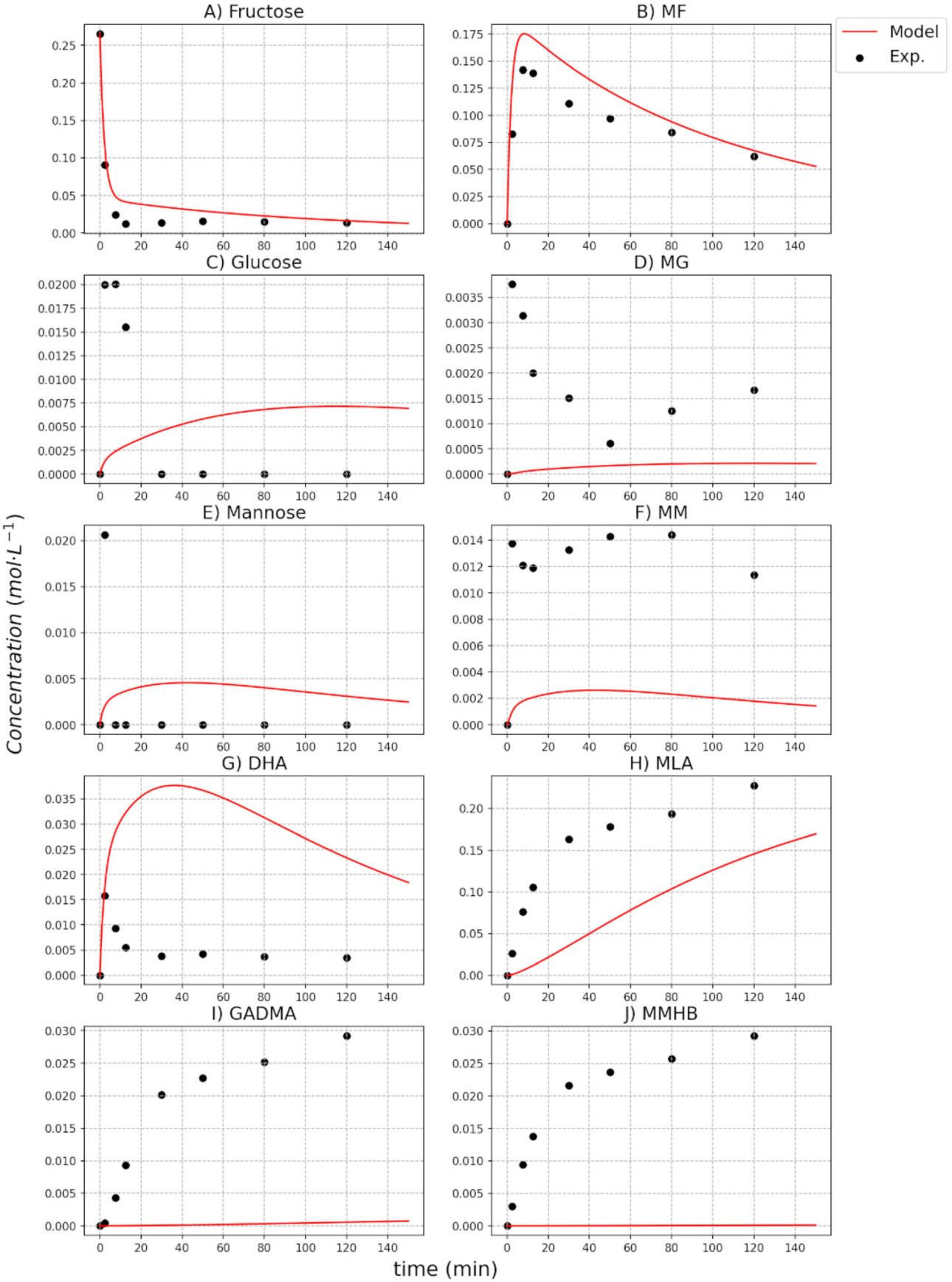

Fig. 7 Validation of the kinetic model at 140 °C when fructose is fed as a substrate. The components presented are A) fructose, B) methyl fructoside (MF), C) glucose, D) methyl glucoside (MG), E) mannose, F) methyl mannoside (MM), G) DHA, H) MLa, I) GADMA and J) MMHB.

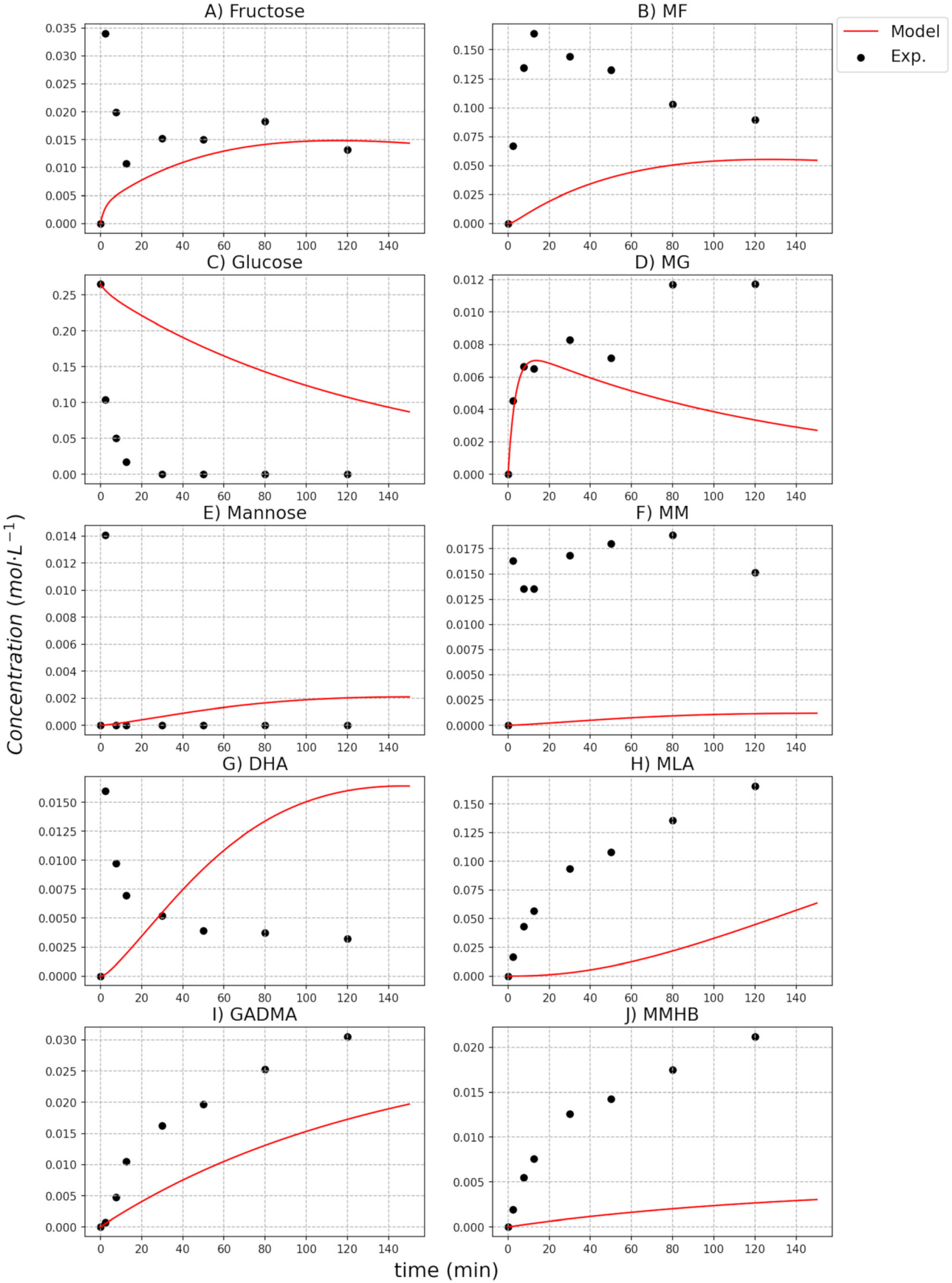

Fig. 8 Validation of the kinetic model at 140 °C when glucose is fed as a substrate. The components presented are A) fructose, B) methyl fructoside (MF), C) glucose, D) methyl glucoside (MG), E) mannose, F) methyl mannoside (MM), G) DHA, H) MLa, I) GADMA and J) CMMHB.

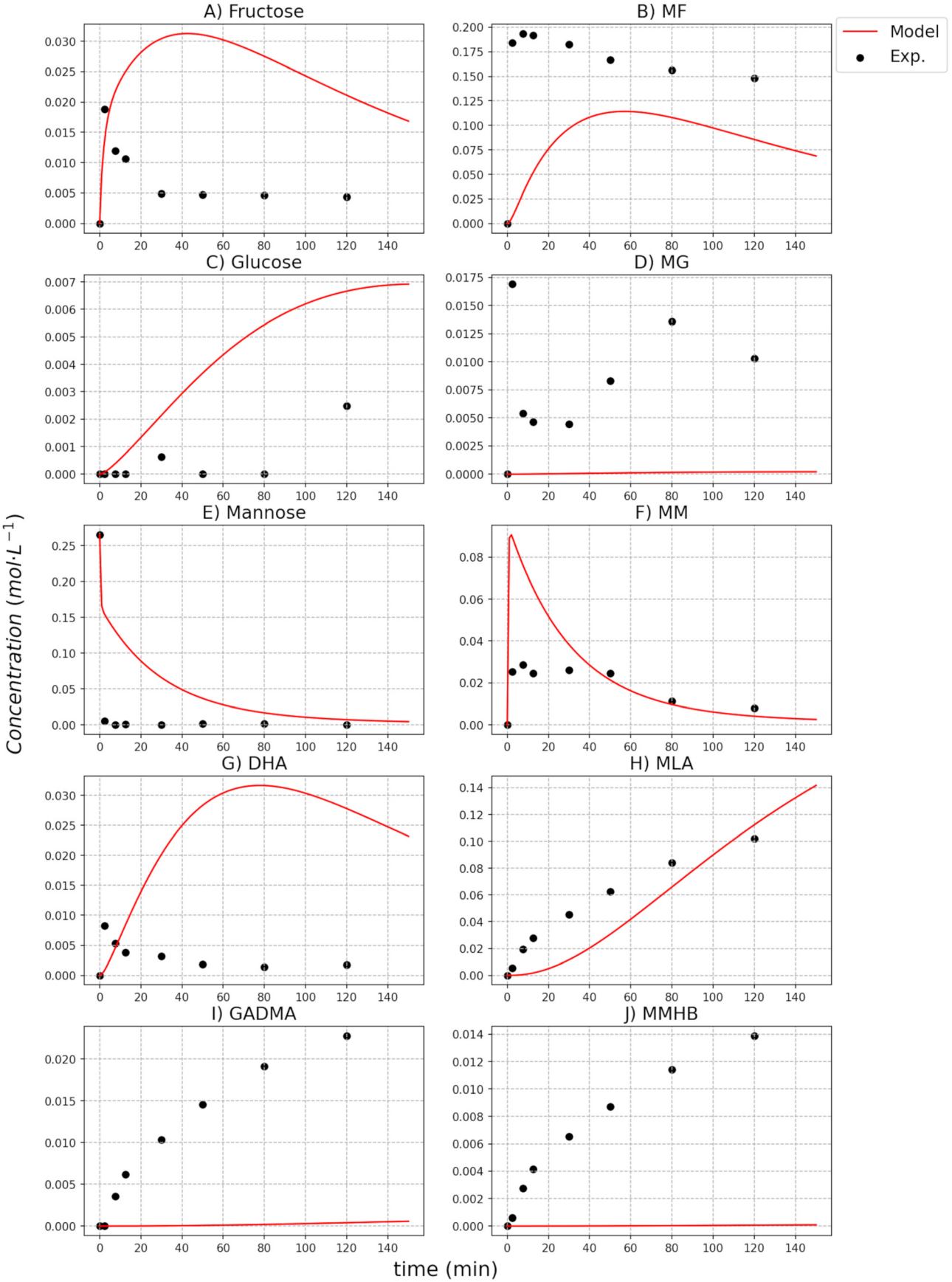

Fig. 9 Validation of the kinetic model at 140 °C when mannose is fed as a substrate. The components presented are A) fructose, B) methyl fructoside (MF), C) glucose, D) methyl glucoside (MG), E) mannose, F) methyl mannoside (MM), G) DHA, H) MLa, I) GADMA and J) CMMHB.

L^{-1}; meanwhile, at high temperatures, the yield is around 35 mol L^{-1}. Thus, the cases at high temperatures have more impact on the minimization of the SSEs.

Conclusions

This work presents a kinetic assessment for the production of methyl lactate with Sn-USY catalysts in methanolic media. The experimental analysis highlights the formation of MMHB and GADMA products through retro-aldol reactions. These reactions were omitted in previous research studies, but they may lead to a yield of 0.06 mol L^{-1} per every mol of the substrate employed. The experimental assessment of the system is completed with the formulation of a kinetic model for simultaneously determining the kinetic and equilibrium parameters of the formation of methyl glycosides, and the side reactions involved in MLa production. The determined kinetic and equilibrium parameters allow us to guess the preferred paths of the reactions and the relevant contributions of each of them. For example, the equilibrium between methyl glycosides and its correspondent sugars was observed to promote the formation of fructose and MF. Similarly, the model provides a guess on the kinetic ratios of the reaction rates and the influence of temperature on them through the Arrhenius equation with its parameters. This is necessary for exploring different reactor designs and optimizing the operating conditions of the reaction. Furthermore, the differences between the kinetic rates of isomerization and methyl glucoside equilibriums are significantly relevant since the current model can be employed for future exploratory analysis of alternative reactants with methyl groups.

Data availability

The data supporting this article have been included as part of the ESI.†

Conflicts of interest

There are no conflicts to declare.

Acknowledgements

This work received financial support from the Spanish Ministry of Science and Innovation through the Cat4BioMon Project (PID2021-122736OB-C44), being funded through MCIN/AEI/10.13039/501100011033/FEDER, UE. This work has received funding from the Bio-based Industries Joint Undertaking (JU) under the European Union's Horizon 2020 research and innovation program under grant agreement 101023202. The JU receives support from the European Union's Horizon 2020 research and innovation program and the Bio-based Industries Consortium.

References

1 M. Moliner, Y. Román-leshkov and M. E. Davis, Tin-containing zeolites are highly active catalysts for the isomerization of glucose in water, *Proc. Natl. Acad. Sci. U. S. A.*, 2010, **107**, 6164–6168, DOI: **10.1073/pnas.1002358107**.

2 C. M. Lew, N. Rajabbeigi and M. Tsapatsis, Microporous and Mesoporous Materials Tin-containing zeolite for the isomerization of cellulosic sugars, *Microporous Mesoporous Mater.*, 2012, **153**, 55–58, DOI: **10.1016/j.micromeso.2011.12.020**.

3 R. Bermejo-deval, R. S. Assary, E. Nikolla, M. Moliner and Y. Román-leshkov, Metalloenzyme-like catalyzed isomerizations of sugars by Lewis acid zeolites, *Proc. Natl. Acad. Sci. U. S. A.*, 2012, **109**, 9727–9732, DOI: **10.1073/pnas.1206708109**.

4 E. Nikolla, Y. Román-Leshkov, M. Moliner and M. E. Davis, "One-Pot" Synthesis of 5-(Hydroxymethyl)furfural from Carbohydrates using Tin-Beta Zeolite, *ACS Catal.*, 2011, **1**, 408–410.

5 K. Saenluang, A. Thivasasith, P. Dugkhuntod, P. Pornsetmetakul, S. Salakhum, S. Namuangruk and C. Wattanakit, In Situ Synthesis of Sn-Beta Zeolite Nanocrystals for Glucose to Hydroxymethylfurfural (HMF), *Catalysts*, 2020, **10**, 1249, DOI: **10.3390/catal10111249**.

6 A. Aho, N. Kumar, K. Eränen, P. Mäki-Arvela, T. Salmi, M. Peurla, I. Angervo, J. Hietala and D. Y. Murzin, Catalytic conversion of glucose to methyl levulinate over metal-modified Beta zeolites, *React. Kinet., Mech. Catal.*, 2022, **135**, 1971–1986, DOI: **10.1007/s11144-022-02225-7**.

7 M. Xia, W. Dong, Z. Shen, S. Xiao, W. Chen, M. Gu and Y. Zhang, Sustainable Energy & Fuels Efficient production of lactic acid from biomass-derived carbohydrates under synergistic effects of indium and tin in In-Sn-Beta zeolites, Sustain, *Energy Fuels*, 2020, **4**, 5327–5338, DOI: **10.1039/d0se00798f**.

8 X. Yang, Y. Zhang, L. Zhou, B. Gao, T. Lu, Y. Su and J. Xu, Production of lactic acid derivatives from sugars over post-synthesized Sn-Beta zeolite promoted by WO3, *Food Chem.*, 2019, **289**, 285–291, DOI: **10.1016/j.foodchem.2019.03.039**.

9 J. Zhang, L. Wang, G. Wang, F. Chen, J. Zhu, C. Wang, C. Bian, S. Pan and F.-S. Xiao, Hierarchical Sn-Beta Zeolite Catalyst for the Conversion of Sugars to Alkyl Lactates, *ACS Sustainable Chem. Eng.*, 2017, **5**, 3123–3131, DOI: **10.1021/acssuschemeng.6b02881**.

10 S. Tolborg, I. Sμdaba, C. M. Osmundsen, P. Fristrup, M. S. Holm and E. Taarning, Tin-containing Silicates: Alkali Salts Improve Methyl Lactate Yield from Sugars, *ChemSusChem*, 2015, **8**, 613–617, DOI: **10.1002/cssc.201403057**.

11 N. Kumar, N. Anil, D. Hazarika, P. Bhagabati, A. Kalamdhad and V. Katiyar, Biodegradation and characterization study of compostable PLA bioplastic containing algae biomass as potential degradation accelerator, *Environ. Challenges*, 2021, **3**, 100067, DOI: **10.1016/j.envc.2021.100067**.

12 P. P. Upare, Y. K. Hwang, J. Chang and D. W. Hwang, Synthesis of Lactide from Alkyl Lactate via a Prepolymer Route, *Ind. Eng. Chem. Res.*, 2012, **51**, 4837–4842, DOI: **10.1021/ie202714n**.

13 A. R. De Clercq, M. Dusselier, E. Makshina and B. F. Sels, Catalytic gas-phase production of lactide from renewable alkyl lactates, *Angew. Chem., Int. Ed.*, 2018, **57**, 3074–3078, DOI: **10.1002/anie.201711446**.

14 L. Tian, Y. Cai, H. R. Alamri, A. M. El-hadi, S. Wu and J. Liu, Effect of initiators on synthesis of poly (L-lactide) by ring opening polymerization Effect of initiators on synthesis of poly (L-lactide) by ring opening polymerization, *IOP Conf. Ser.: Mater. Sci. Eng.*, 2017, **213**, 012022, DOI: **10.1088/1757-899X/213/1/012022**.

15 M. C. D. Alterio, I. D. Auria, L. Gaeta, C. Tedesco, S. Brenna and C. Pellecchia, Are Well Performing Catalysts for the Ring Opening Polymerization of L-Lactide under Mild Laboratory Conditions Suitable for the Industrial Process? The Case of New Highly Active Zn(II) Catalysts, *Macromolecules*, 2022, **55**, 5115–5122, DOI: **10.1021/acs.macromol.2c00719**.

16 P. Van Wouwe, M. Dusselier, E. Vanleeuw and B. Sels, Lactide Synthesis and Chirality Control for Polylactic acid Production, *ChemSusChem*, 2016, **9**, 907–921, DOI: **10.1002/cssc.201501695**.

17 J. Iglesias, I. Martínez-Salazar, P. Maireles-Torres, D. Martin Alonso, R. Mariscal and M. López Granados, Advances in catalytic routes for the production of carboxylic acids from biomass: A step forward for sustainable polymers, *Chem. Soc. Rev.*, 2020, **49**, 5704–5771, DOI: **10.1039/d0cs00177e**.

18 S. Saravanamurugan, M. Paniagua, J. A. Melero and A. Riisager, Efficient Isomerization of Glucose to Fructose over Zeolites in Consecutive Reactions in Alcohol and Aqueous Media, *J. Am. Chem. Soc.*, 2013, **135**, 5246–5249.

19 R. Zhang, A. Eronen, X. Du, E. Ma, M. Guo, K. Moslova and T. Repo, A catalytic approach via retro-aldol condensation of glucose to furanic compounds, *Green Chem.*, 2021, **23**, 5481–5486, DOI: **10.1039/d1gc01429c**.

20 N. Rajabbeigi, A. I. Torres, C. M. Lew, B. Elyassi, L. Ren, Z. Wang, H. J. Cho, W. Fan, P. Daoutidis and M. Tsapatsis, On the kinetics of the isomerization of glucose to fructose using Sn-Beta, *Chem. Eng. Sci.*, 2014, **116**, 235–242, DOI: **10.1016/j.ces.2014.04.031**.

21 I. Tosi, A. Riisager, E. Taarning, P. Rose Jensen and S. Meier, Kinetic Analysis of Hexose Conversion to Methyl Lactate by Sn Beta: Effects of Substrate Masking and of Water, *Catal. Sci. Technol.*, 2018, 2137–2145, DOI: **10.1039/C8CY00335A**.

22 J. Iglesias, J. Moreno, G. Morales, J. A. Melero, P. Juárez, M. López-Granados, R. Mariscal and I. Martínez-Salazar, Sn-Al-USY for the valorization of glucose to methyl lactate: Switching from hydrolytic to retro-aldol activity by alkaline ion exchange, *Green Chem.*, 2019, **21**, 5876–5885, DOI: **10.1039/c9gc02609f**.

23 J. M. Jimenez-Martin, A. Orozco-Saumell, H. Hernando, M. Linares, R. Mariscal, M. López Granados, A. García and J. Iglesias, Efficient Conversion of Glucose to Methyl Lactate with Sn-USY: Retro-aldol Activity Promotion by Controlled Ion Exchange, *ACS Sustainable Chem. Eng.*, 2022, **10**, 8885–8896, DOI: **10.1021/acssuschemeng.2c01987**.

24 F. Pienkoß, C. Ochoa-Hernández, N. Theyssen and W. Leitner, Kaolin: A Natural Low-Cost Material as Catalyst for Isomerization of Glucose to Fructose, *ACS Sustainable Chem. Eng.*, 2018, **6**, 8782–8789, DOI: **10.1021/acssuschemeng.8b01151**.

25 R. N. Goldberg and Y. B. Tewari, Thermodynamics of Enzyme-Catalyzed Reactions: Part 5. Isomerases and Ligases, *J. Phys. Chem. Ref. Data*, 1995, **24**, 1765–1801, DOI: **10.1063/1.555970**.

26 D. M. Gao, T. Kobayashi and S. Adachi, Kinetic analysis for the isomerization of glucose, fructose, and mannose in subcritical aqueous ethanol, *Biosci., Biotechnol., Biochem.*, 2015, **79**, 1005–1010, DOI: **10.1080/09168451.2014.1003129**.

27 P. Li, G. Liu, H. Wu, Y. Liu, J. G. Jiang and P. Wu, Postsynthesis and selective oxidation properties of nanosized Sn-beta zeolite, *J. Phys. Chem. C*, 2011, **115**, 3663–3670, DOI: **10.1021/jp1076966**.

28 R. van Grieken, C. Martos, M. Sánchez-Sánchez, D. P. Serrano, J. A. Melero, J. Iglesias and A. G. Cubero, Synthesis of Sn-silicalite from hydrothermal conversion of SiO2-SnO2 xerogels, *Microporous Mesoporous Mater.*, 2009, **119**, 176–185, DOI: **10.1016/j.micromeso.2008.10.020**.

29 J. M. Jiménez-Martin, M. El Tawil-Lucas, M. Montaña, M. Linares, A. Osatiashtiani, F. Vila, D. M. Alonso, J. Moreno, A. García and J. Iglesias, Production of Methyl Lactate with Sn-USY and Sn-β: Insights into Real Hemicellulose Valorization, *ACS Sustainable Chem. Eng.*, 2024, **12**, 2771–2782, DOI: **10.1021/acssuschemeng.3c07356**.

30 M. Yu, Y. Li, C. Zhang, H. Luo, C. Ge, X. Chen, L. Fu, Z. Ju and X. Yao, Fischer-Helferich glycosidation mechanism of glucose to methyl glycosides over Al-based catalysts in alcoholic media, *RSC Adv.*, 2022, **12**, 23416–23426, DOI: **10.1039/d2ra03945a**.